Identifying Near-Earth Objects on Wide-Field Astronomical Surveys Using a Convolutional Neural Network

Belén Yu Irureta-Goyena Chang
École Polytechnique Fédérale de Lausanne
Elisabeth Rachith
École Polytechnique Fédérale de Lausanne

Jean-Paul Kneib
École Polytechnique Fédérale de Lausanne

ABSTRACT

The present work explores the application of a convolutional neural network to detect moving objects in wide-field astronomical surveys, with a special emphasis on near-Earth objects (NEOs), but also including satellites, space debris, main-belt asteroids, and transneptunian objects (TNOs). The algorithm is developed and tested using images from OmegaCAM, the wide-field camera mounted on ESO's VLT Survey Telescope (VST). The expectation is that the developed tools will also be applicable to a range of other satellite and ground-based surveys, setting the stage for the upcoming generation of telescopes.

The proposed method combines the astronomical software *SourceExtractor* with a machine-learning algorithm. Firstly, *SourceExtractor* is used to detect any sources present on a given image. Secondly, the machine-learning algorithm is applied to determine whether the source is a moving object. The machine-learning algorithm features a convolutional neural network whose architecture is a modified version of the VGG-16 Very Deep Convolutional Network. This model comprises 13 convolutional layers followed by 3 fully connected layers and a rectified linear unit activation function (ReLU) that accounts for non-linearity, an essential feature in image recognition.

Both the adjustment of the hyperparameters of the model and the model training are done using a set of photometric data taken with ESO's VST in Paranal, Chile, under the purview of Programme ID 106.216P.002. In doing this development and to make the procedure more efficient, we also implement physical constraints based on our knowledge of real observing conditions. This programme monitors gravitationally lensed quasars by taking four five-minute exposures in the visible band of the same fields each night. The camera used to take the images is OmegaCAM, a wide-field camera with a field of view of 1 x 1 square degrees. The training set is built by artificially adding tracks of different lengths, orientations and brightness to the VST images.

From its orbit in the L2 Lagrangian point, the upcoming Euclid space mission will also be able to detect moving objects provided a careful analysis of the data collected. These will be essentially main-belt asteroids and transneptunian objects, or even other interstellar objects visiting our solar system, such as 1I/2017 U1 'Oumuamua. With the launch of the Euclid space mission being scheduled for 2023, the Euclid Consortium has developed the software Elvis to generate images similar to those that will be observed during the mission. These simulated images will also be used to further test the applicability of our pipeline on disparate data sets.

Given the wide field of view of the telescopes used (wider than previously used telescopes), we expect to discover objects not yet identified. A catalogue of the detected objects will be produced, analysing trends over the last 10 years, which will be particularly relevant in the case of satellites. In particular, a comprehensive accounting of satellites and space debris in astronomical images will significantly improve the busy eco-system of the Low Earth Orbit, facilitating the coordination of space traffic and reducing the hazard of debris jeopardising space missions. The data will be compared with that available in satellite databases such as Astriagraph.

Furthermore, information on the orbital elements of the detected NEOs will also serve to update the astrometry currently available in dedicated databases such as the Minor Planet Center. Since the astrometry of NEOs remains relatively constant over time, this effort to better characterise it will refine our long-term monitoring of these objects. This will improve our capacity to identify NEOs that may pose a threat to Earth, mitigating local and global damage.

1. INTRODUCTION

The last three decades have seen a strong development in wide-field astronomical surveys. As discussed in [21], they are designed for a variety of purposes, broadly either statistical astronomy [10] or the search of rare objects [20]. However, despite being originally planned for a different purpose, their large field of view makes most of these surveys particularly fit for the detection of moving objects. As a consequence, some of these surveys observe these as secondary products, and some even as their main science objective.

For instance, the Panoramic Survey Telescope and Rapid Response System (Pan-STARRS) [11], located in Hawaii and with a field of view of 3 square degrees, dedicates most of its time to the search of near-Earth objects (NEOs). Similarly, the Zwicky Transient Facility Survey [15], in California, employs a camera with a field of view of 47 square degrees to find asteroids, comets, and supernovae.

In this work, we aim to exploit the data taken with the VLT Survey Telescope (VST) [2]. To the best of our knowledge, such data has not yet been fully explored in search of moving objects. The VST, located in Chile, employs OMEGACAM, a wide-field camera with a field of view of 1 square degree [14]. The long exposure times allow for the detection of a variety of objects moving at different relative speeds, including NEOs, main-belt asteroids and transneptunian objects (TNOs), satellites, and space debris. Our work focuses on the detection of NEOs, but the techniques used are suited for all types of moving objects.

1.1 Near-Earth objects

The term NEO is used to design asteroids — mostly, since it is also applicable to comets — passing close to the orbit of the Earth. Their size can range from metres to tens of kilometres, and they make up around 20,000 of the 600,000 Solar-System objects that we know of [17].

A potential collision of one of these objects with the Earth could cause serious damage. This risk is quantified by the Palermo Technical Impact Hazard Scale [8] and its equivalent made accessible for the general public, the Torino scale [6]. And although the largest NEOs are closely monitored and studied, most small- to medium-sized NEOs, which are also susceptible of causing local damage, remain poorly understood.

Hence, it is essential to build a comprehensive catalogue of NEOs that includes their physical characteristics (such as size and composition) as well as their orbital elements. Since the orbital elements of these objects remain almost constant through time, old data sets can be used to improve our present knowledge.

Furthermore, the study of NEOs can improve our understanding of the Solar System's assembly process.

1.2 Main-belt asteroids and transneptunian objects

The majority of asteroids in the Solar System are located in the main asteroid belt, in-between the orbits of Mars and Jupiter. Their great distance to Earth makes their relative motions much smaller than those of the NEOs, and their pixel imprint is hence shorter. A similar case applies for TNOs, orbiting the Sun beyond the orbit of Neptune, and thus with relative speeds even smaller than the main-belt asteroids.

With a careful analysis, both TNOs and main-belt asteroids can be detected in the VST frames using long exposures. Albeit these objects do not pose the threat of colliding with the Earth, they can also help improving our knowledge of the Solar System.

1.3 Satellites

During the last half a century, the number of artificial satellites has rapidly grown. There are approximately 5,000 active satellites in orbit [13], of which most are located in the Low Earth Orbit (LEO). A statistical analysis over a long period of time can help to identify trends in the satellite population. In addition, unlike the case of asteroids, the orbital elements of the satellites change quickly over time, which implies that to characterise them, fast methods need to be applied to up-to-date data.

1.4 Space debris

However, most of the objects orbiting the Earth are not operative satellites, but space debris created by inactive satellites that either malfunctioned or simply reached the end of their mission and were never retrieved. The estimation is that around 90% of the objects in the LEO are active satellites, a number that increases if the objects smaller than 10 cm are considered.

This growing number is alarming for two reasons: firstly, the debris threatens to collision with active satellites, harming from manned missions to telecommunication satellites; secondly, even if it collides with other space debris, this could lead to a chain reaction, creating more and more collisions. Eventually, as theorised by [12], certain orbits could become so overpopulated that they would be impossible to use for new missions.

Furthermore, since space debris cannot be operated from Earth, it has become much more difficult to extract orbital information about these objects. For this reason, it is key to develop methods to monitor space debris and ensure that this information is used to improve space traffic. Similarly to the case of active satellites, the orbital information of space debris changes quickly, and so efficient methods are required to analyse it.

1.5 State of the art

Multiple studies have studied the detection of moving objects in wide-field images, using data from both space-based and ground-based telescopes.

Among them, one of the most popular methods is perhaps the Hough transform algorithm, which applies a mathematical operation to the input images that yields an output in parameter space. Using a voting system, the algorithm can identify any lines present in the original input, a useful feature for detecting tracks in astronomical images [4]. However, the main disadvantage of the Hough transform is that it needs to be generally optimised for a specific track length. This implies that it can be used to find either short (slow objects) or long (fast objects) tracks, but not both at the same time.

For this reason, the present work focuses on developing machine-learning methods, which are much more versatile than the Hough transform. A similar approach was used by [23], but applied to the ZTF data. The algorithm proposed in this paper builds upon the method developed by Su Direcki at EPFL-LASTRO [9].

2. DATA PRODUCTS

2.1 VST images

For this work, we used images taken with ESO's VLT Survey Telescope (VST) in Paranal, Chile. They were taken under the purview of a programme that monitors gravitationally lensed quasars, with Programme ID 106.216P.002. More specifically, the field used was that of the quasar J1537-3010.

The images were taken with a cadence of four images per night, with an exposure time of 5 minutes per image. The instrument used for this purpose was OmegaCAM, a wide-field camera with a field of view of 1 square degree, which results in images of 16 000$\times$16 000 pixels. Such images are obtained after combining the results of the 32 different CCD cameras that make up the instrument.

2.2 Difference imaging

The technique of difference imaging is commonly used to detect changes between images. In the context of astrophysics, its applications are focused on the the detection of transient objects, either because they are moving (such as asteroids, satellites and space debris) or because they are variable physical objects (variable stars, gravitationally lensed quasars or supernovae). See e.g., [3], [22].

To perform difference imaging, two images of the same field but taken at different times are compared: one called the reference image and the other called the target image. The reference image is usually made by taking the median of several images of that field, often a selection of those with the best seeing. Hence, the reference image will have an optimal point-spread function and no transients present. An example can be seen in Fig. 1.

The target image is our image of interest, where we want to find the astronomical transients. By comparing it with the reference image and subtracting the latter, we can obtain an image that will only contain variable objects.

One of the most challenging aspects of difference imaging is that the point-spread function of the reference image needs to match that of the difference image. To overcome this, a convolutional kernel describing the differences between the two seeings is applied to the reference image. The kernel required needs is usually highly detailed to describe the complex distinctions between the images. For our work, the basis set of the kernel mixes the two most well-known approaches: using individual pixels (proposed by [7]) and using Gaussians of varying widths (proposed by [1]).

To enhance the performance of the convolutional kernel, smaller tiles were cutout from the original mosaic. This ensured that seeing fluctuations across the images were minimised, which simplified the application of the kernel. The mosaics were divided in 100 tiles of size 1768×1768 pixels each. An example of a difference image is shown in Fig. 2.

Our reference images were composed by taking the median of the nine images of the field with the best seeing, as measured by the software *THELI* [18].

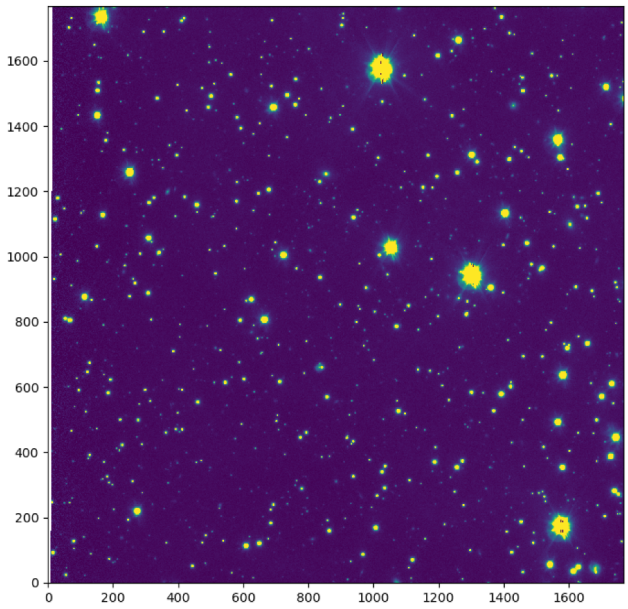

Fig. 1: Reference image.

3. METHODOLOGY

3.1 Data generation

To be able to examine the accuracy of our methods, we needed a data set where the number of moving objects present in the images was fully known. To this end, we used VST images that had been previously processed by the pipeline *THELI*, which contains an algorithm to remove all light tracks.

Subsequently, we artificially injected tracks corresponding to the moving objects into the images. This was done by adding light pixels convolved with the PSF of each difference image. The brightness of the tracks was randomised, although within a range between 3 and 20 times the background noise. The length of the tracks was also randomised from 10 and 1768 pixels, 10 corresponding to the farthest asteroids and 1768 pixels corresponding to satellites crossing the field of view. Most intermediate lengths would correspond to the different types of asteroids described, mainly NEOs and main-belt asteroids. The position and inclination of the tracks was also randomised. Examples of cutouts containing only background noise and containing an artificial track can be seen in Fig. 3 and Fig. 4, respectively.

The method would need to appropriately discern between moving objects and other variable physical objects, such as gravitationally lensed quasars or supernovae. For this purpose, point-like objects were also introduced in the difference images using a similar process: with a brightness between 3 and 20 times the background noise and at random

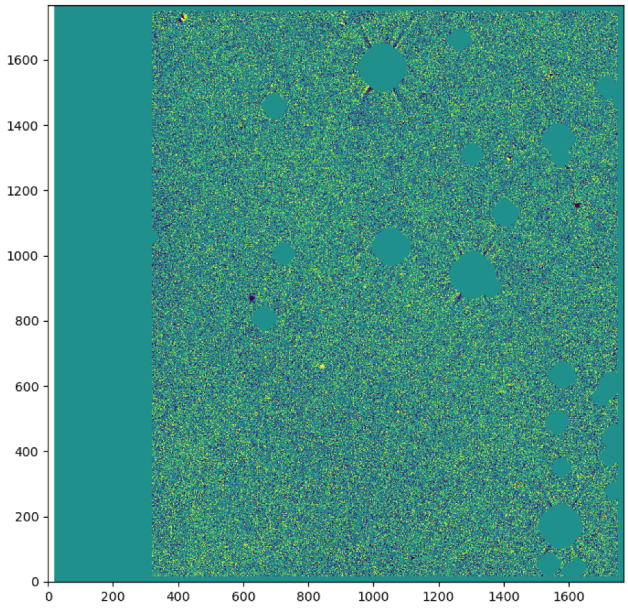

Fig. 2: Difference image.

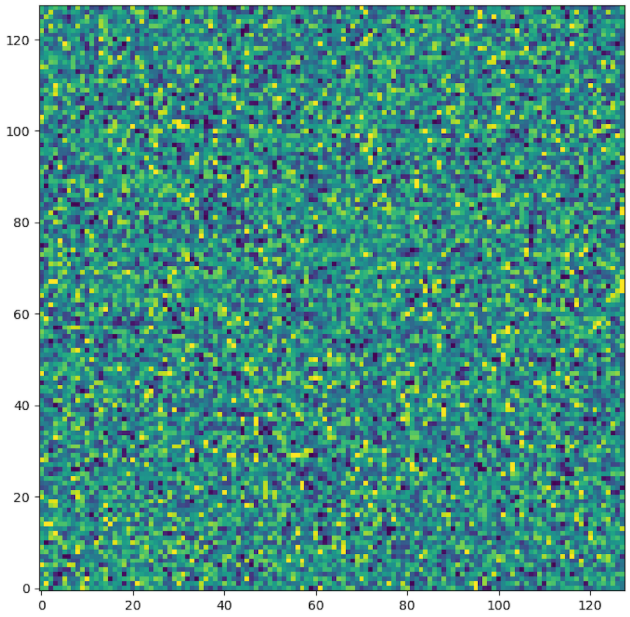

Fig. 3: Cutout with brackground noise.

locations.

3.2 Source detection

Firstly, all the sources in the image were detected using the program *SourceExtractor*. This pipeline identifies all the sources contained within an astronomical image, using several steps: firstly, it builds a background map with a grid covering the frame; secondly, it uses thresholding for an initial detection of the objects; thirdly, it separates blended objects; fourthly, filters the detections, computes their photometry and separates star and galaxy objects. A complete discussion can be found in [5].

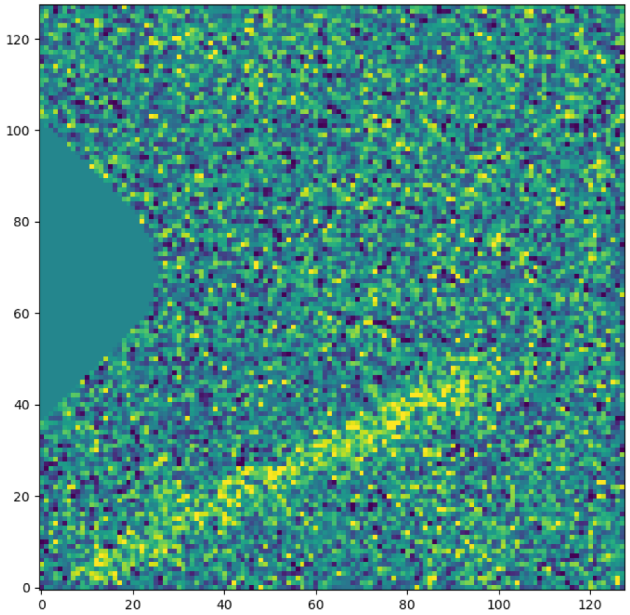

Fig. 4: Cutout with a moving-object track.

A catalogue is built with all the detections found, which will be inversely proportional to the threshold set. Although *SourceExtractor* has the advantage of allowing the user to establish the threshold as low as they like, it presents important limitations. For low thresholds, lower than around 5 times the background noise [16], the software presents a high rate of false positives. Furthermore, and more importantly, it is not optimised to detect very elongated sources, such as the moving objects that concern us. Hence, in our work *SourceExtractor* was only used to create catalogues of all sources present in each difference image.

It is important to mention that some very bright elements in the reference image will overexpose the pixels around them but not necessarily in the target image, and vice versa. Therefore, when creating the difference image, this will introduce 'fake sources' in it. To mitigate this effect, *SourceExtractor* was also used to build a catalogue of the reference image, which was then compared to that of the difference image. All the sources in the difference image adjacent to sources in the reference catalogue, and hence likely to be overexposed pixels, were removed.

Then, all detections that belonged to the same object were grouped using agglomerative hierarchical clustering. The bottom-up method `fclusterdata` was used, since these type of methods are robust when the ideal number of clusters is not known. After clustering, a centroid was assigned to each resultant cluster, calculated by weighting all points by their flux and taking the mean. Subsequently, a tile around the centroid was cut out, of size 128×128 pixels.

3.3 Source identification

After detecting the sources with *SourceExtractor* and cutting smaller tiles around them, we applied a convolutional neural network to discern whether they belong to a moving object (track) or not.

To this end, a VGG-16 architecture was used, which is a deep convolutional network for large-scale image recognition [19]. In short, this type of algorithm can learn to classify an image according to a binary metric. In this case, it yielded the probability that the a cutout contained a track or not.

This model had two advantages: firstly, it was more adaptable to different track lengths than the Hough transform, which, as discussed, is only optimised for a certain type of track; secondly, it was robust against any contamination from overexposed pixels that were not handled in the previous step.

The model was trained using 33 728 cutouts with dimensions 128×128, labeled into two groups: 33.33% containing a moving-object track and 66.66% only containing point-objects or background noise. The model was trained using the Adam optimizer, dropout and class weights.

3.4 Source characterisation

Once the tracks were correctly identified by the neural network, a second step was performed by the network to determine where in the cutout the moving objects was located. In other words, which pixels belonged to a track and, in particular, which point was most likely to be the centre of the track.

This procedure was done by applying the model to smaller tiles centered around each point. With this, we could select the cutout that had been predicted by the model to contain a light track with the highest confidence. Lastly, a Hough-transform elipse-fitting algorithm was used to calculate the orientation of the track.

4. RESULTS

The results obtained using our pipeline will be described in this section.

Once the cutouts had been identified, the convolutional neural network was able to correctly detect the tracks in 62% of the cases. This number was calculated by applying the model to 1000 cutouts, out of which 30% contained tracks and 70% contained background noise or point sources.

To visualise this source-identification step in conjunction with the source-detection and source-characterisation steps, the full pipeline was tested on several 1768×1768 images. An example is shown in Fig. 5:

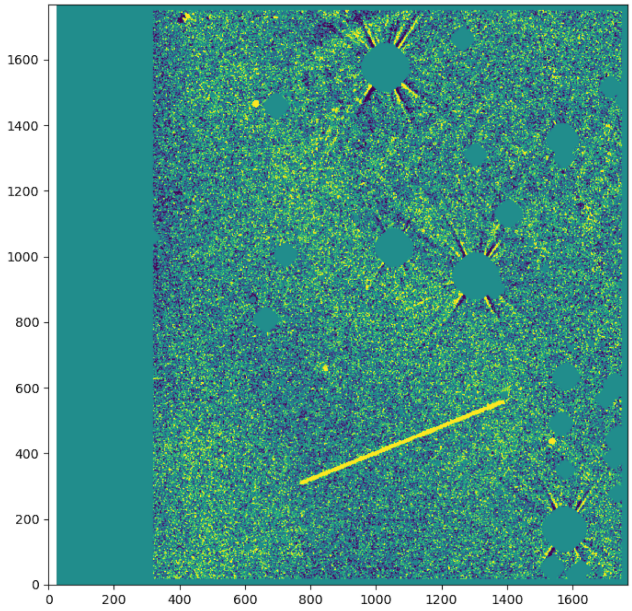

Fig. 5: Example of an image with added track and point sources.

This image contains a track corresponding to a moving object and 4 point sources that represent various physical phenomena.

Firstly, *SourceExtractor* was applied to build a catalogue of the difference image, which yielded 9 detected sources, as shown in Fig. 6.

Then, the same software was applied to the reference image, and a reference catalogue was built. Both catalogues were compared and the points in the difference catalogue close to sources detected in the reference catalogue were discarded, as discussed in Section 3. This reduced the number of detections to 7. The remainder of the sources in the difference image were then clustered into 5 cutouts, which were fed to the convolutional neural network. The model, as shown in Fig. 7, correctly detected that 2 of them were part of moving-object tracks, and also discarded the point sources.

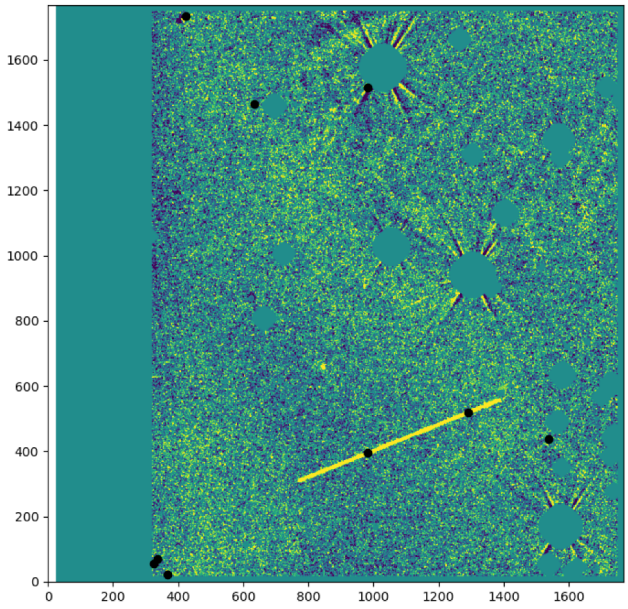

Fig. 6: Detections of *SourceExtractor*.

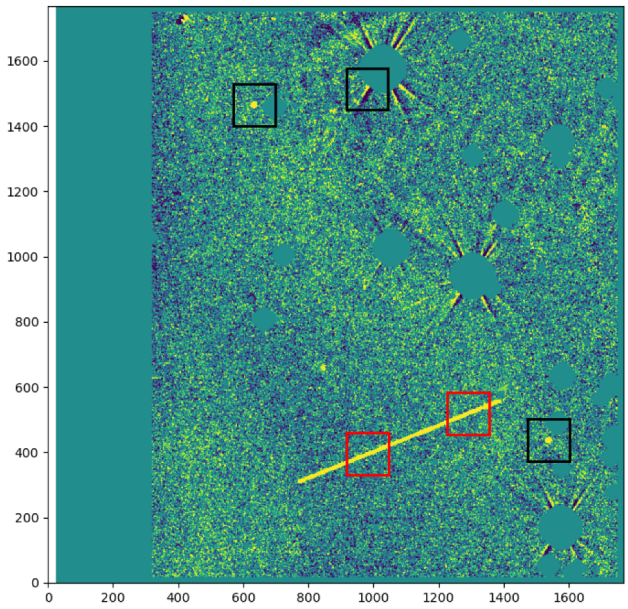

Fig. 7: Cutouts fed to the convolutional neural network. Cutouts identified as containing tracks are shown in red.

Lastly, the orientation of the track was calculated by fitting a Hough-transform algorithm. The computed orientation was 22°, which was close to the true value, 27°. However, more points of the track would be needed to improve this estimation.

5. CONCLUSION

The present work applied a convolutional neural network to a set of images taken with the wide-field, VST telescope with the objective of identifying moving objects, particularly near-Earth asteroids. Firstly, any sources were detected

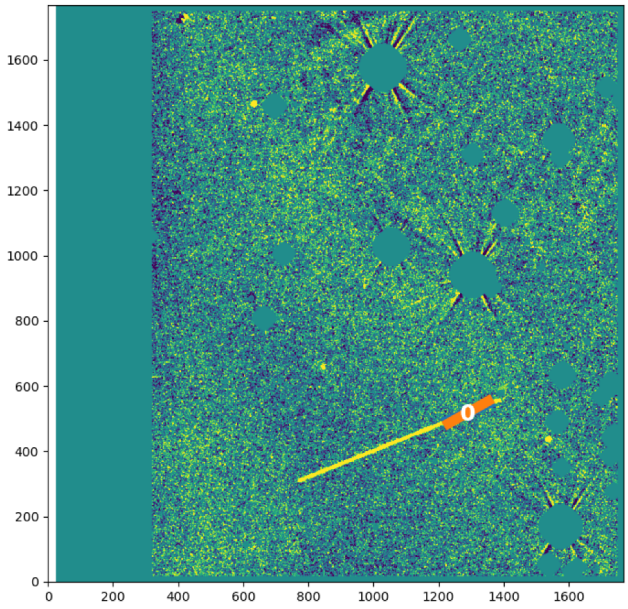

Fig. 8: Orientation fit with the Hough transform algorithm.

using the software *SourceExtractor*. Secondly, they were grouped into clusters and fed to the model, which identified whether they belonged to the track of a moving object. Thirdly, the objects were characterised by computing the orientation of their track.

Moving forward, our work will focus on improving the accuracy of the model. To this end, it will be retrained using a larger, more diverse data set. We believe that the brightness 3 times the background noise might be too low for the convolutional neural network to meaningfully discern the images. For this reason, we will try building a new data set with brighter objects and retraining the model.

After the model is optimised, we will apply the method described to a set of VST images that do not have artificial tracks in them, and check how many moving objects can be identified. Any detections will be reported to the Minor Planet Center and Astriagraph databases, and compared with those currently in the catalogues.

Another change that will be implemented in the future pipeline is to use images from the same night to build the reference image. The reason behind this is that some telescopes, such as the upcoming mission Euclid, will not observe the same field over multiple nights. Hence, we propose using the median of the four different exposures of a particular that are taken each night to create the reference image. The difference image would be made by using each individual exposure as a target frame and performing the subtraction with the reference frame. The seeing of the two being almost the same, a convolutional kernel would probably not be necessary in this case.

Lastly, we will focus on further characterising the objects detected, by computing not only the orientation of the tracks, but also other physical variables such as their speed.

ACKNOWLEDGEMENTS

I would like to thank Dr Cameron Lemon and Dr Stephan Hellmich for all their useful advice and comments. This project has received funding from the European Union's Horizon 2020 research and innovation programme under the Marie Sklodowska-Curie grant agreement No 945363.

6. REFERENCES

[1] Christophe Alard. Image subtraction using a space-varying kernel. *Astronomy and Astrophysics Supplement Series*, 144(2):363–370, 2000.

[2] Magda Arnaboldi, Massimo Capaccioli, Dario Mancini, Roberto Scaramella, Giorgio Sedmak, and Richard Kurz. The vst-vlt survey telescope. In *From Extrasolar Planets to Cosmology: The VLT Opening Symposium*, pages 204–208. Springer, 2000.

[3] Stephen Bailey, Cecilia Aragon, Raquel Romano, Rollin C Thomas, Benjamin A Weaver, and Daniel Wong. How to find more supernovae with less work: Object classification techniques for difference imaging. *The Astrophysical Journal*, 665(2):1246, 2007.

[4] Pascal Ballester. Hough transform and astronomical data analysis. *Vistas in Astronomy*, 40(4):479–485, 1996.

[5] E. Bertin and S. Arnouts. SExtractor: Software for source extraction. *Astronomy and Astrophysics Supplement Series*, 117(2):393–404, June 1996.

[6] Richard P Binzel. The torino impact hazard scale. *Planetary and Space Science*, 48(4):297–303, 2000.

[7] D. M. Bramich. A new algorithm for difference image analysis. *Monthly Notices of the Royal Astronomical Society: Letters*, 386(1):L77–L81, May 2008.

[8] Steven R. Chesley, Paul W. Chodas, Andrea Milani, Giovanni B. Valsecchi, and Donald K. Yeomans. Quantifying the risk posed by potential earth impacts. *Icarus*, 159(2):423–432, October 2002.

[9] S. Direkci. Studies on satellite detection with difference imaging, 2020.

[10] Brenna Flaugher. The dark energy survey. *International Journal of Modern Physics A*, 20(14):3121–3123, June 2005.

[11] Nicholas Kaiser. Pan-STARRS: a wide-field optical survey telescope array. In Jr. Jacobus M. Oschmann, editor, *SPIE Proceedings*. SPIE, September 2004.

[12] Donald J. Kessler. Collisional cascading: The limits of population growth in low earth orbit. *Advances in Space Research*, 11(12):63–66, January 1991.

[13] D. G. King-Hele. *A Tapestry of Orbits*. 1992.

[14] K Kuijken, R Bender, E Cappellaro, B Muschielok, A Baruffolo, E Cascone, O Iwert, W Mitsch, H Nicklas, EA Valentijn, et al. Omegacam: the 16k× 16k ccd camera for the vlt survey telescope. *The Messenger*, 110:15–18, 2002.

[15] Frank J. Masci, Russ R. Laher, Ben Rusholme, David L. Shupe, Steven Groom, Jason Surace, Edward Jackson, Serge Monkewitz, Ron Beck, David Flynn, Scott Terek, Walter Landry, Eugean Hacopians, Vandana Desai, Justin Howell, Tim Brooke, David Imel, Stefanie Wachter, Quan-Zhi Ye, Hsing-Wen Lin, S. Bradley Cenko, Virginia Cunningham, Umaa Rebbapragada, Brian Bue, Adam A. Miller, Ashish Mahabal, Eric C. Bellm, Maria T. Patterson, Mario Jurić, V. Zach Golkhou, Eran O. Ofek, Richard Walters, Matthew Graham, Mansi M. Kasliwal, Richard G. Dekany, Thomas Kupfer, Kevin Burdge, Christopher B. Cannella, Tom Barlow, Angela Van Sistine, Matteo Giomi, Christoffer Fremling, Nadejda Blagorodnova, David Levitan, Reed Riddle, Roger M. Smith, George Helou, Thomas A. Prince, and Shrinivas R. Kulkarni. The zwicky transient facility: Data processing, products, and archive. *Publications of the Astronomical Society of the Pacific*, 131(995):018003, December 2018.

[16] Guy Nir, Barak Zackay, and Eran O. Ofek. Optimal and efficient streak detection in astronomical images. *The Astronomical Journal*, 156(5):229, October 2018.

[17] D Perna, MA Barucci, and M Fulchignoni. The near-earth objects and their potential threat to our planet. *The Astronomy and Astrophysics Review*, 21(1):1–28, 2013.

[18] M. Schirmer. THELI: Convenient Reduction of Optical, Near-infrared, and Mid-infrared Imaging Data. , 209(2):21, December 2013.

[19] Karen Simonyan and Andrew Zisserman. Very deep convolutional networks for large-scale image recognition, 2015.

[20] BT Soifer, JR Houck, and G Neugebauer. The iras view of the extragalactic sky. *Annual Review of Astronomy and Astrophysics*, 25(1):187–230, 1987.

[21] Michael A. Strauss, J.Anthony Tyson, Scott F. Anderson, T.S. Axelrod, Andrew C. Becker, Steven J. Bickerton, Michael R. Blanton, David L. Burke, J.J. Condon, and A.J. Connolly. Wide-field astronomical surveys in the next decade. Technical report, March 2009.

[22] Andrzej Udalski. The optical gravitational lensing experiment. real time data analysis systems in the ogle-iii survey. *arXiv preprint astro-ph/0401123*, 2004.

[23] Quanzhi Ye, Frank J. Masci, Hsing Wen Lin, Bryce Bolin, Chan-Kao Chang, Dmitry A. Duev, George Helou, Wing-Huen Ip, David L. Kaplan, Emily Kramer, Ashish Mahabal, Chow-Choong Ngeow, Avery J. Nielsen, Thomas A. Prince, Hanjie Tan, Ting-Shuo Yeh, Eric C. Bellm, Richard Dekany, Matteo Giomi, Matthew J. Graham, Shrinivas R. Kulkarni, Thomas Kupfer, Russ R. Laher, Ben Rusholme, David L. Shupe, and Charlotte Ward. Toward efficient detection of small near-earth asteroids using the zwicky transient facility (ZTF). *Publications of the Astronomical Society of the Pacific*, 131(1001):078002, May 2019.